Sensors & Actuators: A. Physical 384 (2025) 116255

Contents lists available at ScienceDirect

Sensors and Actuators: A. Physical

journal homepage: www.journals.elsevier.com/sensors-and-actuators-a-physical

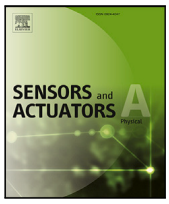

Design of SMA wire based actuators: A phase transformation and electric coupling parametric study

Marcos Lopes Leal Júnior [a,b,c,*], Laurent Pino [a], Mahmoud Barati [b,c,d], Luc Saint-Sulpice [a], Laurent Daniel [b,c], Shabnam Arbab Chirani [a]

[a] ENI Brest, UMR CNRS 6027, IRDL, F-29200, Brest, France
[b] Université Paris-Saclay, CentraleSupélec, CNRS, Laboratoire de Génie Électrique et Électronique de Paris, 91192, Gif-sur-Yvette, France
[c] Sorbonne Université, CNRS, Laboratoire de Génie Électrique et Électronique de Paris, 75252, Paris, France
[d] EMITECH Group, 78180, Montigny-le-Bretonneux, France

ARTICLE INFO

Keywords:
Shape Memory Alloys
Actuator design
Electric activation
Thermomechanical coupling
Macroscopic model
Activation parameters

ABSTRACT

New strategies for the design of Shape Memory Alloy (SMA) actuators are needed to fill the gap between their high potential and limited industrial implementation. This gap stems from a number of challenges, such as the need for robust methods to predict and track their thermomechanical behavior under varying operational conditions, the lack of tools to model and mitigate functional fatigue during cycling, and the absence of systematic design frameworks that take into account the complex interdependencies of activation parameters. In this regard, this work proposes a straightforward strategy for designing SMA wire actuators based on parametric simulations of their thermomechanical behavior. The influence of key activation parameters, including heating time, cooling time, electrical current, axial stress, and wire diameter, on SMA actuator performance is investigated by focusing on initial actuation strain and maximum operating temperature. An experimental study is performed to explore the interdependencies of these parameters and their impact on the actuator behavior. On this basis, a new parametric analysis method is proposed to identify optimal actuation parameters for various operating conditions. The method consists of a three-step approach. Each step focuses on different aspects of the SMA actuation (e.g. activation conditions, SMA dimensions and SMA cyclic behavior) that together address the majority of imposed industrial specifications.

1. Introduction

Despite the great potential for using Shape Memory Alloys (SMA) as actuators in industrial context (e.g. automotive), it is scarcely implemented [1]. Major reasons for this are the insufficient knowledge of the thermomechanical behavior under operational conditions, the lack of designing methods and the lack of understanding of the properties degradation upon cycling, also known as Functional Fatigue (FF) [2–7].

During the actuation, the phase transformation is triggered by the heating and cooling process under mechanical loading. For the heating stage, two main techniques are employed to heat up the SMA component: external heating and electrical or Joule heating. The latter is widely adopted over the former due to its higher heating rate and easier implementation (no need for additional equipment and the possibility of being powered by portable batteries) [8,9]. Nevertheless, the use of an electric drive makes control and use more challenging due to the electro-thermal-mechanical coupling nature. In this way, the phase transformation and consequently the actuation becomes dependent on the adjustment and control of several parameters related to the power supply.

When considering electrical heating, parameters controlling the amount of energy passing through the SMA component drives the actuation. In light of this, some affecting parameters can be listed: the heating time HT (period during which the electric current passes through the SMA component), the cooling time CT (period without electric current), the maximum voltage U, the maximum current i, the SMA component resistance R (defined by the SMA dimensions), the global resistance R_T (when more than one SMA component are considered) and the current waveform (e.g., sine, square, and ramp signal) [5,10]. These parameters compose the activation setup of the SMA actuators. It is worth noting that the electric resistance of SMAs is not constant during an actuation cycle and varies with the metallurgical state and with temperature evolution. The effect of the microstructure and temperature on the electric resistance has been addressed in [11–15]. Other features can externally impact the actuator's operation. For

* Corresponding author.
E-mail address: marcosleal_00@hotmail.com (M. Lopes Leal Júnior).

https://doi.org/10.1016/j.sna.2025.116255
Received 23 September 2024; Received in revised form 19 December 2024; Accepted 21 January 2025
Available online 29 January 2025

Nomenclature

π^t	Thermodynamic forces conjugate to ξ
$\rho^{electric}$	Total electric resistivity
σ	Axial mechanical stress
σ_{crit}	Critical stress below which $H^{cur} = H^{min}$
ε, ε^{tr}, ε^{r}, ε^{el}, ε^{th}	Uniaxial total, transformation, residual, elastic, thermal strain
ε^{tr}	Transformation strain
ε_0^{tr}	Initial actuation strain
$\varnothing$	SMA wire diameter
ξ	Martensitic volume fraction
A^t	Set of internal state variables
A_s, A_f	Austenitic phase transformation start and finish temperatures at zero stress
A_{wire}	Cross section area of the wire
c	Specific heat
CT	Cooling time
d	Diameter
G	Gibbs free energy potential
g^t	Transformation hardening energy
h	Convection coefficient
h	Heat convection coefficient
H^{cur}, H^{min}	Max. and Min. saturation current transformation strain
H^{sat}	Saturation current transformation strain
HT	Heating time
i	Maximum current
k	Exponential evolution rate coefficient
L	Length of the specimen
M_s, M_f	Martensitic phase transformation start and finish temperatures at zero stress
q	Heat flux
R	SMA component electric resistance
r	Internal heat generation rate
R_s, R_f	R-phase transformation start and finish temperatures at zero stress
R_T	Global resistance
s	Mass-specific entropy
T	Temperature
T_0, s_0, u_0	Temperature, mass-specific entropy, specific internal energy at the reference state
T_{amb}	Room temperature
T_{lim}	Temperature threshold to guarantee no SMA overheating
T_{max}	Maximum operating temperature
U	Maximum voltage
u	Mass-specific internal energy
V_{wire}	Volume of the wire

instance, reset components, external mechanisms and actuation control devices are equally employed to control, improve and/or adapt the actuator output [16,17].

Given the great number of activation parameters, countless settings can be obtained for an identical actuator output. The specification of this set of parameters is not straightforward since they are strongly coupled. For instance, slight changes in the current intensity may imply a significant variation in actuation time ($HT + CT$), when similar

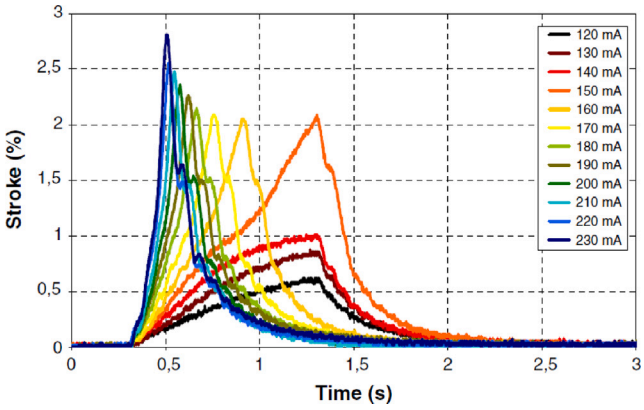

Fig. 1. Heating time and actuation stroke of a SMA wire actuator for currents from 120 to 230 mA.
Source: Adapted from [20].

output (force and stroke) is considered [18,19]. One of these non-linear relationships has been experimentally studied in [20] as presented in Fig. 1. In addition, it is possible to note that for some configurations, the SMA is heated too quickly which may result in overheating and thereby, damage [21,22]. On the other hand, when the heating is too slow, only a fraction of the stroke is produced which indicates that the phase transformation was not correctly initiated or completed.

In addition to activation parameters, other aspects related to the cooling process can impact the actuator performance. Most frequently, the SMA component is cooled via heat exchange through natural or forced air convection [23]. For this, different exchange fluids (air, water, or other fluid) can be selected depending on the application specifications. Due to the small size of the majority of SMA-based actuators, natural convection through air is the most employed solution. In this regard, two related parameters can be highlighted: the ambient temperature and the cooling method. The former is generally a non-controllable parameter and strongly depends on the environment conditions. The latter is chosen according to the temperature differential between the hottest and coolest actuation points, exchange surface and amount of material to be cooled (depending on the SMA dimensions).

Addressing this complex issue, several studies have explored coupled models to tackle the multiphysics nature of the problem. [24] proposed a finite-element modeling approach to simulate SMA phase transformations while incorporating variable thermal and mechanical properties. Subsequently, [25–27] introduced similar methodologies, utilizing one-dimensional constitutive models thermally coupled to predict or control SMA actuator displacements. While these approaches exhibit strong alignment with experimental results, they often overlook the influence of dynamic effects associated with high electrical current levels. In contrast, [28] presented an energetic framework that integrates stored thermal energy, latent heat, and thermal losses, providing a more accurate simulation for scenarios involving rapid actuation. Additionally, [19] extended this concept through the Brinson constitutive model, incorporating broader experimental foundations. Although these methods address diverse experimental conditions, selecting optimal electrical parameters remains a challenging task. To address this, [18] conducted numerical investigations to identify optimized electrical conditions for designers. However, the proposed modeling techniques face limitations, particularly in extending to three-dimensional formulations and considering cyclic behaviors, including FF aspects. The cyclic behavior of SMAs exhibits significant variations under constant loading conditions [2,29]. This evolution also referred to as FF, is detrimental to some actuator applications. Consequently, it is imperative to consider the degradation of the SMA behavior in order to respect the industrial requirements.

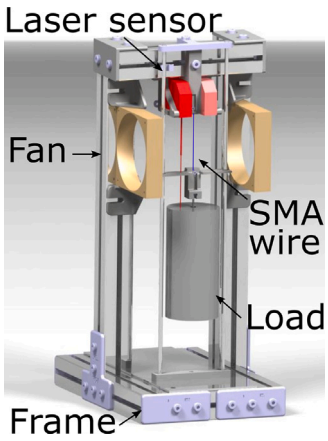

Fig. 2. CAD representation of the *ad hoc* fatigue testing machine.

In summary, the influence of various parameters on actuation is highly diverse, with some parameters exhibiting strong interdependencies while others are not controllable. These conditions contribute to a complex and challenging scenario for accurate prediction and simulation. Moreover, well-known FF symptoms such as the reduction of the transformation strain amount and the evolution of the phase transformation temperatures — mainly attributed to Residual Stress-Induced Martensite (RSIM) [30,31] and Transformation Induced Plasticity (TRIP) accumulation [4,32,33] - further exacerbate in the designing SMA actuators.

The goal of this work is to propose a new method for designers to conceive SMA actuators. This method is mainly based on a parametric analysis that can predict the most adaptable set of actuation parameters for a given application by using an electric-thermal-mechanical coupled modeling approach that also accounts for FF aspects related with SMA actuation, presented in [34]. For such an evaluation the parameter CT, HT, σ (axial stress), i and $\varnothing$ (wire diameter) are considered to evaluate the SMA actuator initial performance in terms of produced stroke (estimated through the initial actuation strain ε_0^{tr}), developed force (through the σ value) and maximum operating temperature (T_{max}).

The work is organized as follows. An experimental analysis of the influence of some activation parameters on a SMA wire response is presented in Section 2. Then, a design method based on a parametric analysis is proposed and detailed in Section 3. The simulation results of the parametric analysis are presented and validated in Section 4. The final remarks follow in Section 5.

2. Experimental analysis

An *ad hoc* testing machine (presented in Fig. 2) was designed to reproduce the diverse actuation scenarios using a wide range of HT, CT, i and σ levels. In the following, the experimental conditions are detailed, then the analysis of the impact of some activation parameters on the initial amount of transformation strain produced is regarded. Finally, the temperature distribution along a SMA wire during a cycle is assessed.

2.1. Experimental conditions

Dynalloy® (DN) wires of two distinct diameters were selected for experimental testing. Specifically, ⌀0.20 mm wires were used for analyzing maximum transformation strain and conducting correlation analysis, while ⌀0.38 mm wires were employed for temperature distribution studies and model calibration. Additionally, a third set of ⌀0.50 mm wire was included solely for parametric analysis. Table 1 summarizes the applications of each wire diameter across the various areas of investigation. For each experimental test, a new 90 mm long specimen was employed. Each specimen was hand-prepared by using a mounting guide to uniformly attach the wires to a metallic crimp. Fig. 3 shows some specimens and their typical dimensions.

Table 1
Considered DN wires and performed analysis.

	Diameter, ⌀ [mm]		
	0.20	0.38	0.50
Experimental analysis			
Maximum transformation strain	X		
Temperature distribution		X	
Modeling analysis			
Calibration		X	
Impact of different parameters	X		
Validation	X		
Practical example	X	X	X

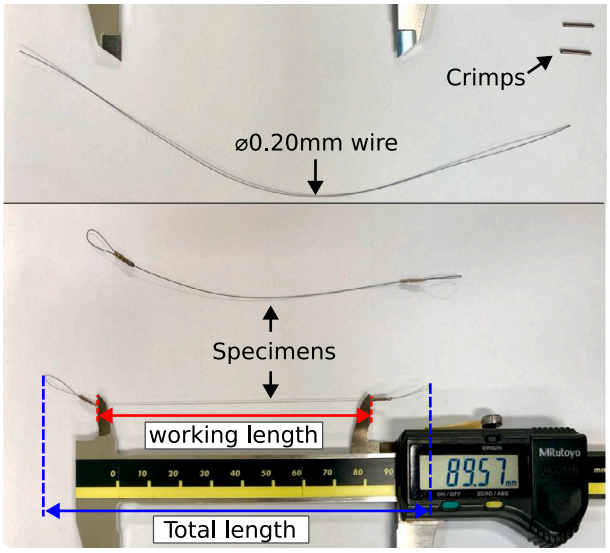

Fig. 3. NiTi wires and prepared specimens. The Caliper measurement indicates the working length of the specimen (the length of material that generates work). The total length of the specimen is also indicated by blue arrows.

During the experiments, the SMA wires are heated using Joule effect, cooled by two electric commanded fans and mechanically loaded via a dead weight. The SMA mechanical response was measured by two laser sensors pointed to a target plate, positioned at the same height as the end of the SMA wire. This target plate is also the support part that electrically powers the wire and holds the dead weight. The imposed electric conditions were monitored through an *ad hoc* program and recorded by sensors placed on a control board. To minimize noise during the measurements, the power supplies for the measurement devices and for the SMA wire were set distinctly, as shown in Fig. 4.

Additionally to the mechanical behavior, the thermal response of the actuator is also measured. An Infrared (IR) camera was employed to evaluate the temperature evolution of wires surface. To ensure correct temperature estimations, the emissivity coefficients of the employed wires was evaluated in a separate dedicated experiment and then employed in the experimental procedure.

Firstly, three stress levels and two input current levels were considered. The stress values (100, 230 and 340 MPa) were chosen according to the indication of the wire manufacturer: 100 MPa is the stress for which the produced residual strain under cycling is considered minimal, 230 MPa is considered the maximum stress to ensure 100k cycles and 340 MPa is the yield stress at high temperatures [23]. Secondly, a wide range of HT, CT values was tested for all diameters, stress

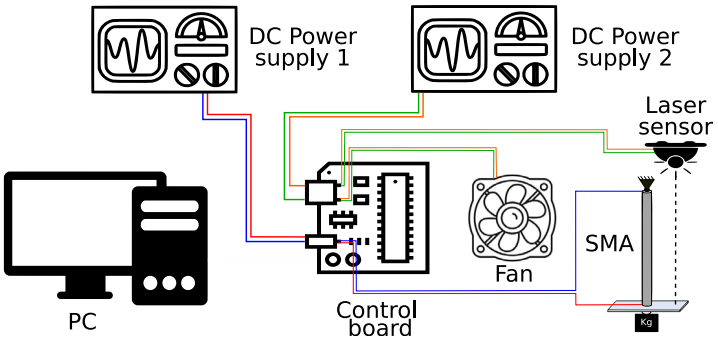

Fig. 4. Electric circuit of the *ad hoc* testing machine.

Table 2
Testing conditions for the initial actuation strain analysis with ∅0.20 mm wires.

Max. current, i [A]	Stress, σ [MPa]	Heating time range, HT [s]	Cooling time, CT [s]
1.0	100	0.55–1.00	2
	230	0.50–1.00	2
	340	0.56–0.80	2
1.5	100	0.18	2
	230	0.20–0.24	2
	340	0.25–0.30	2

and current levels in the preliminary study to ensure ϵ_0^{tr} greater than 2.0% (herein considered minimum output strain for an actuation) and compliance with a commonly employed actuation frequency restriction: $HT + CT < 3$ s.

For each test, the experimental data were processed and the initial transformation strain and temperature parameters analyzed. In the following, the actuator behavior during initial cycles is examined.

2.2. Influence of the experimental parameters on the initial actuation strain

For the initial transformation strain analysis, ϵ_0^{tr} was evaluated by averaging the transformation strain ϵ^{tr} for the first twenty actuation cycles. This is necessary because during the very first cycles (1 to 10), the SMA wire average temperature is not stabilized yet. Therefore, averaging ϵ^{tr} over 20 cycles allows reducing uncertainties on ϵ_0^{tr} estimation. The implemented loading conditions are given in Table 2.

First, the impact of HT on ϵ_0^{tr} is investigated by analyzing Fig. 5. Fig. 5(a) shows that for similar ϵ_0^{tr} values, the needed amount of HT is different depending on the stress level. This observation is in agreement with the stress-temperature slopes identified in Appendix and with the Clausius-Clapeyron relation indicating that the required temperature (herein controlled by HT) to trigger the phase transformation depends on the stress level. Moreover, the presented ϵ_0^{tr} vs. HT relationship at each stress level shows a saturating curve with a maximum ϵ_0^{tr} value. This behavior can be explained by the fact that at lower HT values, the provided electric energy is not sufficient for triggering the phase transformation. Then, at a specific HT value, the reached energy is enough to transform the material and transformation strain is produced. From this point, ϵ^{tr} evolves rapidly with HT until a point at which the material produces its maximum transformation and remains at this level. Finally, it is expected that ϵ^{tr} starts to decay due to the insufficient cooling time (CT set constant) for the wire to transform back to martensitic state, therefore, less phase transformation occurs.

Second, Fig. 5(b) shows that the required HT to produce a certain ϵ_0^{tr} decreases when the current increases. This is an expected behavior, as the produced heat depends on the generated electric power ($P = i.U$). However, it is also noted that the ϵ_0^{tr} vs. HT relationship is not linear within the studied range. In fact, ϵ_0^{tr} appears to evolve in an exponential form with HT. Therefore, one may conclude that ϵ_0^{tr} is mainly impacted by HT and also depends on σ and i.

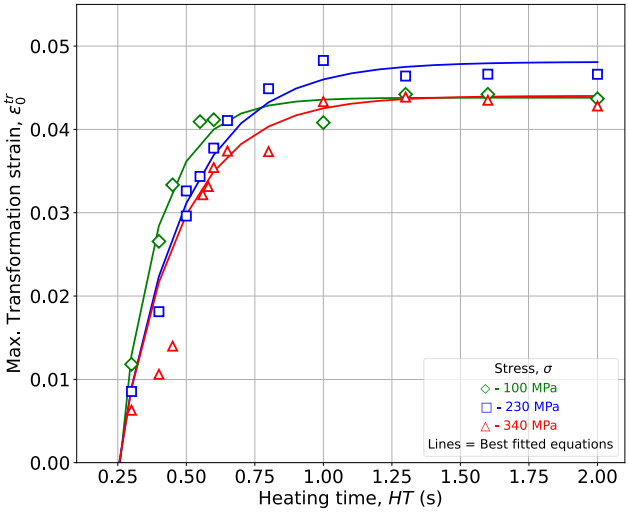

(a) ϵ_0^{tr} as function of HT under fixed current level (i =1 A).

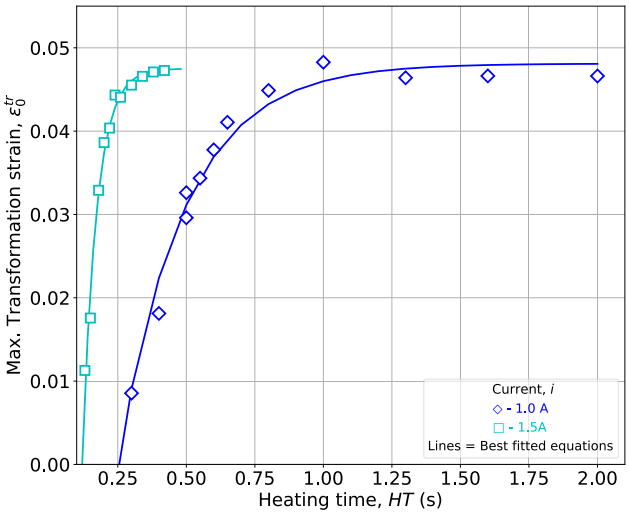

(b) ϵ_0^{tr} as function of HT for two current levels at σ=230 MPa.

Fig. 5. Impact of the HT on the ϵ_0^{tr} under different levels of stress and current and fixed CT for ∅0.20 mm wires.

Considering that ϵ_0^{tr} is an important parameter when designing SMA actuators (related to the actuator stroke), having a function that is capable of estimating ϵ_0^{tr} for given HT, σ and i is required. However, as aforementioned, the relationship between these three parameters has

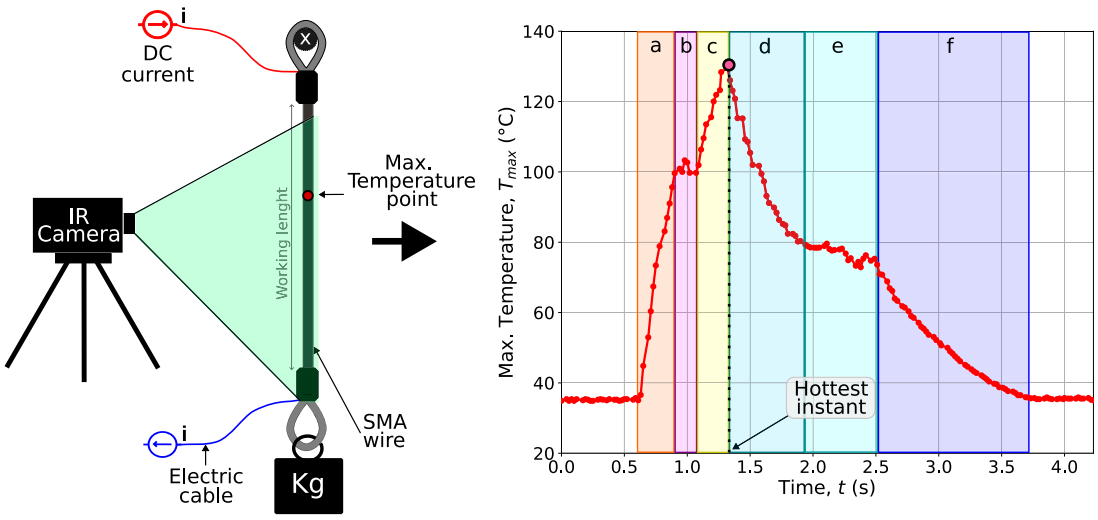

Fig. 6. Representation of the SMA wire temperature measurement by infrared camera (left) and the maximum temperature response during one cycle (right). The letters a to f in the Maximum temperature vs. time graph denote the six different temperature rate zones which are colored. (For interpretation of the references to color in this figure legend, the reader is referred to the web version of this article.)

shown to be complex. For this reason, a numerical approach is proposed. Before moving to the method description, the thermal response is analyzed in the following.

2.3. Temperature distribution along the wire

In order to analyze the thermal response and the temperature distribution along the ∅0.38 mm wire (which presented a more precise thermal response in comparison with the ∅0.20 mm one), an additional apparatus was employed for the experimental observations. An IR thermal camera was used to record the temperature along almost the entire working length. Two different experimental observations were obtained from the measurements: the thermal response at the hottest point during all the total actuation time (shown in Fig. 6) and the temperature distribution along the wire length at the hottest instant (shown in Fig. 7).

Regarding the thermal response of the hottest point on the right side of Fig. 6, it can be divided into six zones (a, b, c, d, e and f). The first zone (a) corresponds to an almost linear temperature evolution in time. This behavior is associated with the wire's heating under constant electric power. Then, the temperature evolution changes abruptly to a very low or null rate during a short period (b zone). The decrease in temperature rate is associated with the reverse phase transformation (martensite to austenite state) which is endothermic and consumes a part of the delivered electric power to the wire. Next, another almost constant temperature evolution rate starts and lasts until the end of HT. In this zone (denoted c), no phase transformation occurs. During the cooling stage, the temperature evolution rates are the same as for the heating one. Zone d: free cooling, zone e: cooling under forward phase transformation (austenite to martensite state) and zone f: free cooling to room temperature. The presented thermal response is typical of Joule heating under constant load. This behavior has also been reported in [35,36].

With respect to the temperature profile along the wire length (Fig. 7), the observed temperatures are not constant and seem to vary in an oscillatory way along the wire. The reason for this profile form may be linked to the phase transformation localization phenomenon and/or to the forced cooling flow. However, no further investigation was performed on this subject, due to experimental limitations. Furthermore, the difference between the hottest and coolest point is about 18 °C, which can be considered low, regarding the maximum reached temperatures. Thus, it can be inferred that the temperature profile along the wire length is almost homogeneous.

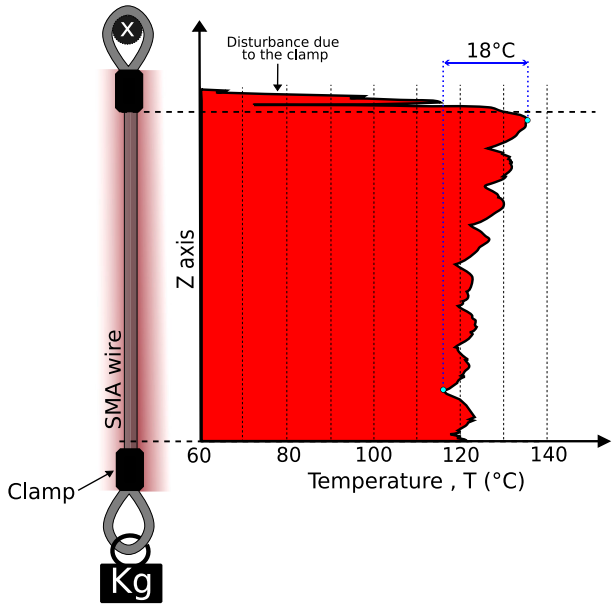

Fig. 7. Temperature profile along the wire length at the hottest instant (end of heating phase).

In short, the experimental investigations demonstrated that the impact of σ, i and HT on the initial actuation strain is non-linear. In addition to the non-linearity, the initial activation strain also depends on the other factors, proving the strongly coupled character of the actuation parameters in SMA actuation.

3. Designing SMA actuators

In this section, a modeling strategy accounting for the cyclic thermomechanical behavior of SMA-based actuators activated by Joule heating is considered. This strategy considers a weak coupling method to address the multiphysics complexity as comprehensively described in [34]. Based on this framework, a detailed methodology for designing SMA actuators is subsequently introduced. The procedure includes a parametric analysis to investigate and clarify the impact of the principal input parameters (HT, CT, i, ∅) on the actuator thermomechanical

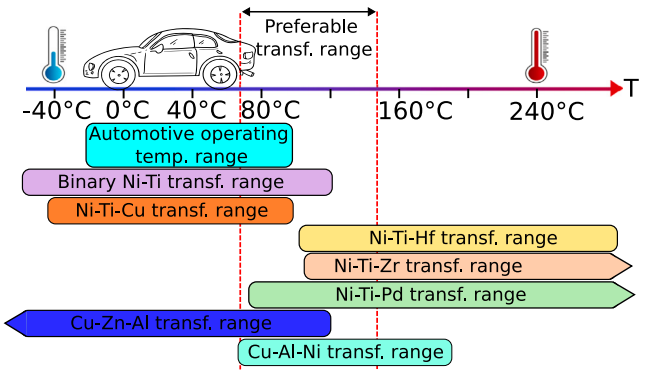

Fig. 8. Operating temperature range for automotive applications and the transformation temperatures for some commercially available SMAs.
Source: Adapted from [1].

behavior.

For the design method, a three-step approach is proposed. It accounts for the SMA composition selection, activation conditions and dimensions and SMA cyclic behavior simulation. In the following, each of these steps is described.

3.1. SMA composition selection and experimental characterization

The most important factors for SMA actuator design can be categorized as inherent and external. The inherent factors are related to the SMA properties and depend on the composition and thermomechanical treatment (e.g., training procedure). Thus, once the SMA composition is selected, these characteristics do not change. Based on this, the design method starts with the selection of the SMA composition to preset the operating conditions. It is worth noting that for standard actuation applications, NiTi alloys are recommended [1,17,37].

The SMA selection is performed by considering the operating temperature range in which the actuator is used. For instance, Fig. 8 compares different compositions of SMA component with respect to the operating conditions of automotive applications. This material choice defines the phase transformation temperatures of the SMA. Then, the desired displacement is regarded and linked to the maximum transformation strain (H^{cur}), which is also dependent on the SMA composition. As introduced in [38], the maximum transformation strain rises with an exponential form as the stress increases and can be expressed by the equation $H^{cur} = H_{min}+(H_{sat}+H_{min})(1-e^{-k(\sigma-\sigma_{crit})})$. In order to obtain the necessary data, an experimental characterization procedure including Differential Scanning Calorimetry (DSC), Assisted Shape Memory Effect (ASME) and Superelastic (SE) experiments must be performed.

At this step, in addition to the composition, the quantity of SMA components is defined. Based on the required output force and maximum and minimum loading conditions (typically provided by the manufacturers as in [23]) it is possible to evaluate if more than one component is necessary for the force requirements.

3.2. Activation conditions and SMA dimensions

Once most of the inherent parameters are defined, this second step focuses on the external ones. The objective is to define the activation conditions and the SMA wire dimensions (diameter and length).

Considering the coupled nature of problem, an analysis based on a parametric evaluation is recommended to define the best conditions. Given the available wire diameters for the chosen SMA composition and the maximum length of the wire (specified by the dimensional restrictions), parametric evaluations return to the designer different sets of activation conditions that would generate the desired output (force and stroke). Then, a preselection of the proposed sets must be performed considering the operational restrictions (power supply limitations and actuation frequency). These operational conditions will likewise define the SMA component length range through the consideration of specific electric resistance and power supply limitations.

At this point, other current actuator configurations for associated devices (e.g. dead weight and bias springs) and cooling methods (e.g. forced air, oil immersion and others) can also be considered in the parametric evaluations [16,17].

At the end of this step, sets of activation conditions and SMA dimensions are proposed for the SMA actuator.

3.3. SMA behavior simulation

The last step is the simulation of the SMA behavior in actuation context. At this stage, one set of activation conditions is considered together with the SMA properties and dimensions. The objective is to achieve precise simulations of the thermomechanical behavior of SMA during its entire operational lifespan. To this end, the proposed approach also incorporates the simulation of FF aspects, which can significantly modify the actuator performance. Examples of such effects are discussed in [34]. While the adopted modeling approach is capable of capturing these phenomena, this aspect is not addressed in this work and requires further investigation to ensure the proper actuator operation over its full lifespan. To give the reader a visual reference of the proposed method, a flowchart is presented in Fig. 9.

In the proposed approach, the first step can be accomplished without major difficulties from some experimental tests and analysis of the manufacturers data sheet. The last step, that treats the cyclic behavior of such actuators was already examined in [34]. Consequently, the remaining obstacle to design the SMA actuator is the second step, related to the choice of activation parameters. In the following section, this second step is further described and some results are analyzed to complete the description of the design method.

4. Parametric analysis

Before explaining the parametric procedure, some of the most important features of the employed constitutive modeling strategy are recalled. The employed numerical strategy consist of a resolution based on the works of [39,40]. It employs a modified one-dimensional version of the constitutive SMA model of [34,41,42] that uses the Gibbs free energy potential written as a function of the applied stress σ and absolute temperature T as external state variables and A^t as the set of internal state variables associated with the inelastic transformation process: G(σ, T, A^t). The set of internal state variables A^t is chosen as $A^t = \left(\varepsilon^{tr}, \varepsilon^r, \xi, g^t\right)$, where the transformation strain ε^{tr} is the inelastic strain generated during phase transformation; the residual strain ε^r is the inelastic strain associated to (RSIM) and also contains (TRIP) contributions; the martensitic volume fraction ξ accounts for the generation and recovery of all martensitic variants and varies between $0 \leq \xi \leq 1$; and the transformation hardening energy g^t is a measure of the change in mixing energy. Thus, the Gibbs free energy is decomposed in three components:

$$G\left(\sigma, T, \varepsilon^{tr}, \varepsilon^r, \xi, g^t\right) = (1-\xi)G^A(\sigma, T) + \xi G^M(\sigma, T) + G^{mix}\left(\sigma, \varepsilon^{tr}, \varepsilon^r, g^t\right), \tag{1}$$

where G^γ accounts for the thermoelastic free energy associated to pure states ($\gamma = A$ or M) and G^{mix} corresponds to a mixing energy term.

The total strain partition is given by:

$$\varepsilon = \varepsilon^{el} + \varepsilon^{th} + \varepsilon^{tr} + \varepsilon^r, \tag{2}$$

where ε^{el} and ε^{th} corresponds to the elastic and thermal strain terms.

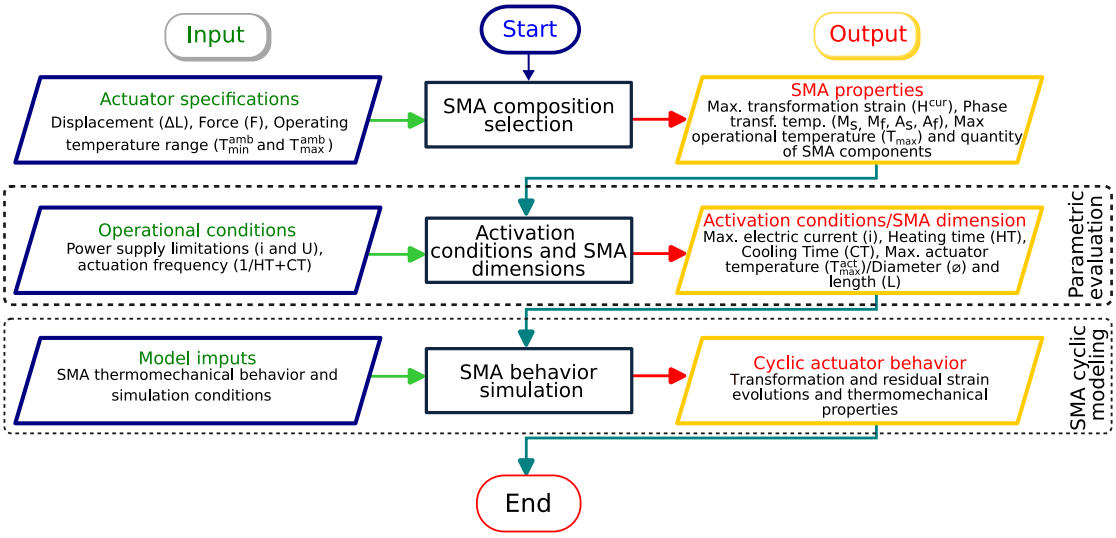

Fig. 9. Design method for SMA wire actuators.

To deal with the thermomechanical coupling and the intrinsic dissipation contributions, the equilibrium equation of heat can be reduced to :

$$T\alpha\dot{\sigma} - \rho c\Delta T + \left(-\pi^t + \rho\Delta s_0 T\right)\Delta\xi = q(T) + \rho r, \tag{3}$$

The parameters ρ and α denote the density and the thermal expansion therms, respectively, and are assumed to be phase-independent. The other given parameters (c, s_0, π^t and r) are the specific heat capacity (assumed equal for both austenite and martensite phases), specific entropy at the reference state, the effective thermodynamic driving force for transformation, the specific heat source/sink term, respectively. The therm $q(T)$ denotes the heat flux vector for a heat transfer problem through convection for a circular cross-section under one-dimensional assumptions and is given by :

$$q(T) = -\frac{A_{wire}}{V_{wire}}h(T - T_{amb}) = -\frac{4h}{d}(T - T_{amb}), \tag{4}$$

where h is the heat convection coefficient, d is the diameter of the considered wire, A_{wire} and V_{wire} are the surface and the volume of the wire, respectively, and T_{amb} is the room temperature.

The modeling strategy accounts for a weak coupling method, used to resolve the partial differential equations sequentially. The strategy is divided into three stages: electrical analysis which considers the electric current input and the heat exchange with the surroundings via convection; thermo-elastic prediction which accounts for the heat generated in the previous stage; and SMA thermomechanical analysis which uses a return mapping algorithm (RMA) [43] to evaluate and correct the phase transformation parameters. For the electrical analysis, the total electrical energy provided to the actuator is considered to be completely converted into heat. Thus, the added energy in the system is considered as the heat source/sink term in Eq. (3). To evaluate this term, the density of heat (q_c) developed by DC current (i) passing through a homogeneous conductor is expressed as [44]:

$$q_c = \frac{i^2 R}{V_{wire}}, \tag{5}$$

The electrical resistance can also be expressed as:

$$R = \frac{\rho^{electric} L}{A_{wire}}, \tag{6}$$

where, $\rho^{electric}$ is the electrical resistivity of the wire, here considered as temperature and martensite volume fraction dependent ($\rho^{electric} = \rho^{electric}(\xi, T)$). L is the total length of the wire actuator. Substituting Eq. (6) into Eq. (5) we obtain the density of heat as a function of electrical resistivity.

$$q_c = \frac{\rho^{electric} L}{A_{wire}}\frac{i^2}{V_{wire}} \Rightarrow q_c = \rho^{electric}\left(\frac{4i}{\pi d^2}\right)^2. \tag{7}$$

The previous equation can be expressed as the heat source/sink term:

$$\rho r = \rho^{electric}\left(\frac{4i}{\pi d^2}\right)^2. \tag{8}$$

The selected model has shown to be capable of reproducing both initial and cyclic behavior of electrically activated SMA wires. As demonstrated in [34], some typical features such as the temperature plateau and the sensitivity to electric current intensity are correctly simulated. Therefore, this model can be employed in parametric analysis to investigate the initial performance of SMA actuators. In addition, the model is also able to simulate the aspects linked to functional fatigue, an important feature that can be incorporated into the analysis.

In this analysis, simulations of a plethora of actuation conditions are considered in a parametric approach: two actuation parameters are incrementally modified during the investigation. First, the impact of the total actuation time is studied (with HT and CT varying), then the impact of the electric activation (with HT and i varying) and lastly, the impact of the wire diameter (with HT and i varying for three wire diameters). In each case, the actuator response is investigated through the analysis of ϵ_0^{tr} and T_{max}, that together, can describe the actuator performance.

To ensure coherent and accurate simulations, the model calibration was carried out before the parametric evaluation.

4.1. Model calibration

For this first step in the parametric analysis, the model calibration was performed with ⌀0.39 mm wires, which presented a better thermal resolution when using IR temperature measurements. For the calibration procedure, loading conditions of $\sigma = 275$ MPa, $HT = 0.50$ s and $CT = 3.0$ s were selected. The employed material properties and the corresponding characterization tests are given in Appendix. The analyzed parameters in this simulation are the temperature and strain evolution during 10 cycles. The comparisons between experimental and simulation results are presented in Figs. 10 and 11.

At given electric current input profile, the temperature and strain simulations demonstrated a good agreement with the experimental data. For the two first cycles, a bigger disparity is observed for the maximum temperature and strain. Then, for the following cycles, the model

Table 3
Testing conditions for parametric analysis with ∅0.20 mm wires.

	Max. current, i [A]	Stress, σ [MPa]	Heating time range, HT [s]	Cooling time, CT [s]
Actuation time analysis	1.0	230	0.15:0.05:1.00	0.3:0.1:2
Electric activation analysis	0.60:0.05:1.5	100	0.10:0.075:1.30	2

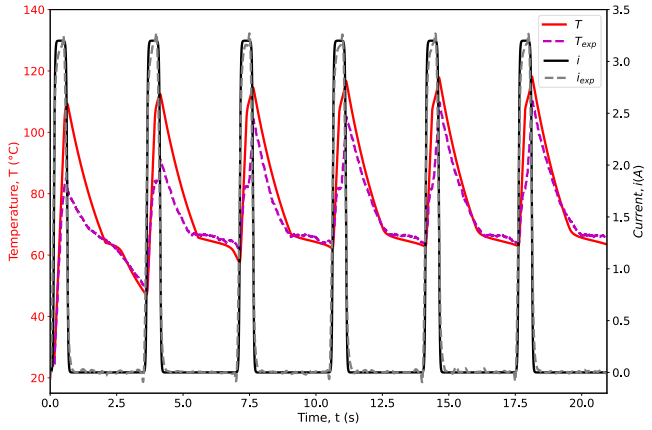

Fig. 10. Comparison between the simulated and the experimental results for the temperature and current response during two actuation time periods for a ∅0.38 mm wire. The model curves are shown in plain lines and the experimental ones in dashed lines.

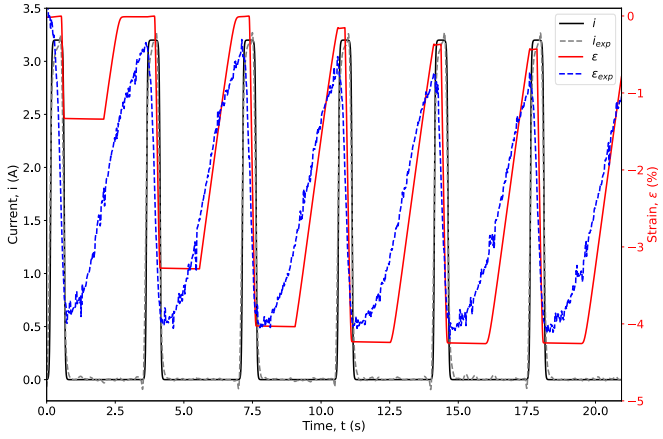

Fig. 11. Comparison between the simulated and the experimental results for the total strain and current response during two actuation time periods for a ∅0.38 mm wire. The model curves are shown in plain lines and the experimental ones in dashed lines.

results converges to a very similar actuator response. The temperature plateaus are well represented in the simulations and good correspondences with the phase transformation temperatures are achieved. However, as already discussed in [34], due to the consideration of one single integration point, the model is not capable of describing the smooth evolution of the produced strain. This is due to the heterogeneity of the phase transformation process over the SMA wire length. Despite this drawback, the temperature and strain amplitudes are well described and the model is considered calibrated.

After ensuring that the simulations are consistent with the SMA wire dynamics, parametric analysis were performed. They are presented in the following sections.

4.2. Impact of the total actuation time

For the two following parametric analysis, in order to cross-verify the accuracy of the simulations, ∅0.20 mm diameter wires were employed. The considered parametric conditions are compiled in Table 3.

First, investigations on the impact of the total actuation time ($HT + CT$) on ε_0^{tr} and T_{max} are conducted. All material parameters and the input parameters were set constant except for HT and CT. The considered loading condition was set as $\sigma = 230$ MPa, $i = 1$ A and $T_{amb} = 25$ °C. The actuation times were set varying in the following ranges: 0.15 s to 1.0 s with a step of 0.05 s for HT and from 0.3 s to 2.0 s with a step of 0.1 s for CT. The simulation results for each configuration were extracted at the 10th cycle, which is considered to exhibit a stabilized average temperature. The results are shown in a two-dimensional contour graph with the colors representing the isocurves of the analyzed output.

Fig. 12 shows that the relationship between HT and CT is not linear for both investigated outputs. Regarding ε_0^{tr} (Fig. 12(a)), three important points can be highlighted. First, a minimal CT is required to trigger the phase transformation. Moreover, the minimal CT value evolves exponentially with HT for each ε_0^{tr} isovalues. Second, the minimal HT to ensure phase transformation can be determined by graph analysis. Once the minimal HT is ensured, it can be observed that ε_0^{tr} is very sensitive to the slightest change in CT. For instance, at $HT = 0.8$ s, a slight variation in CT (between 0.35 s and 0.55 s) leads to a very significant increase in ε_0^{tr}. Third, when considering isotime values (diagonal lines), it is noted that, only a very narrow set of $HT + CT$ corresponds to a given ε_0^{tr} value. In other words, when total actuation time is imposed for the actuator, finding the desired ε_0^{tr} output can be very difficult, especially for small total actuation time.

When examining T_{max}, the relationship between HT and CT changes considerably in comparison with ε_0^{tr}. First, T_{max} is mostly impacted by HT and minimally by CT, this slight impact originating from the thermomechanical coupling (effect of latent heats). Second, for a given total actuation time, the set of parameters ensuring a given T_{max} value is wider than for ε_0^{tr}, which facilitates the temperature control.

4.3. Impact of the electric activation

Following the same strategy, the impact of the electric activation is now addressed. For this analysis, the most important electrical parameters (HT and i) were considered. HT range was set from 0.10 s to 1.30 s with steps of 0.075 s and i from 0.60 A to 1.50 A with steps of 0.05 A. The remaining parameters were set constants for all the considered conditions, and CT defined as 2 s. The results of the parametric simulations are shown in Fig. 13.

First, when analyzing ε_0^{tr}, the relationship between HT and i is not linear and, once more, they correlate in an exponential form. Moreover, the transition between minimal and maximal ε_0^{tr} is very narrow for each current level. This means that the produced amount of ε_0^{tr} is very sensitive to both HT and i.

Next, when evaluating T_{max}, the reached temperatures vary greatly in the considered activation range. Under lower current (0.6~1.1 A), the temperature hardly evolves with the heating time increase. On the other hand, when higher currents are set, e.g. 1.4 A, slight changes in HT increase significantly the maximum temperature. Therefore, the proposed analysis is essential to the design of the actuator, especially regarding the maximum reached temperatures. T_{max} must be accurately controlled to avoid overheating and malfunctioning.

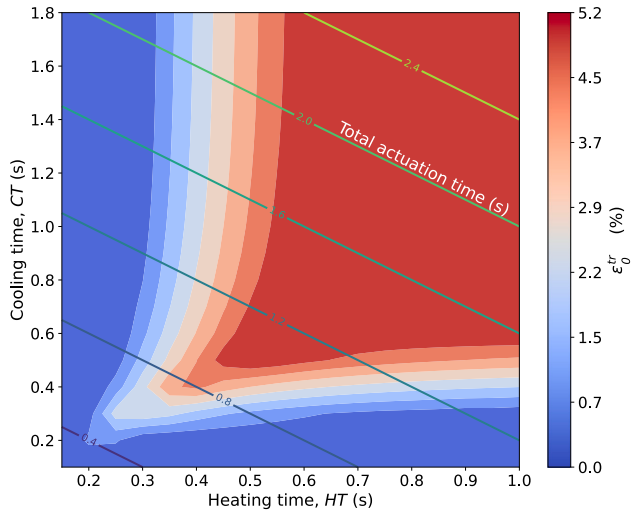

(a) ε_0^{tr} isocurves.

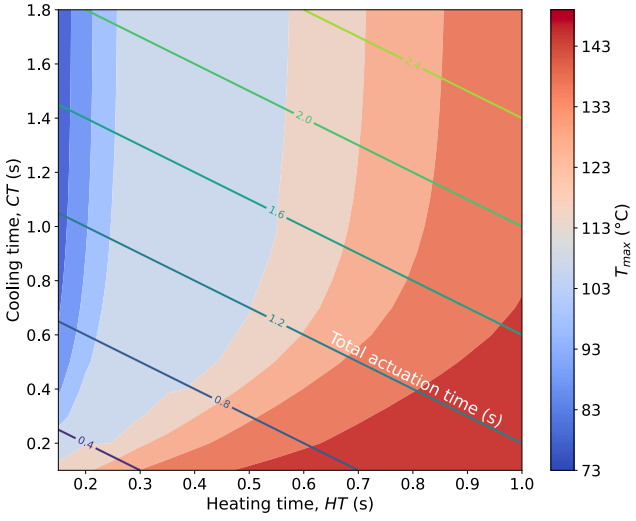

(b) T_{max} isocurves.

Fig. 12. ε_0^{tr} and T_{max} isocurves for different sets of total actuation time for the ∅0.20 mm wire. The inclined lines represent the isovalues for the total actuation time. The color bars at the right side indicate the maximum transformation strain for figure (a) and the maximum reached temperature for figure (b) after ten actuation cycles. (For interpretation of the references to color in this figure legend, the reader is referred to the web version of this article.)

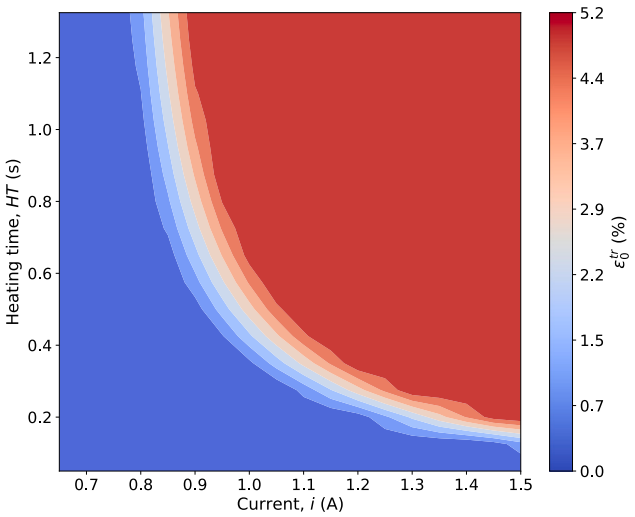

(a) ε_0^{tr} isocurves.

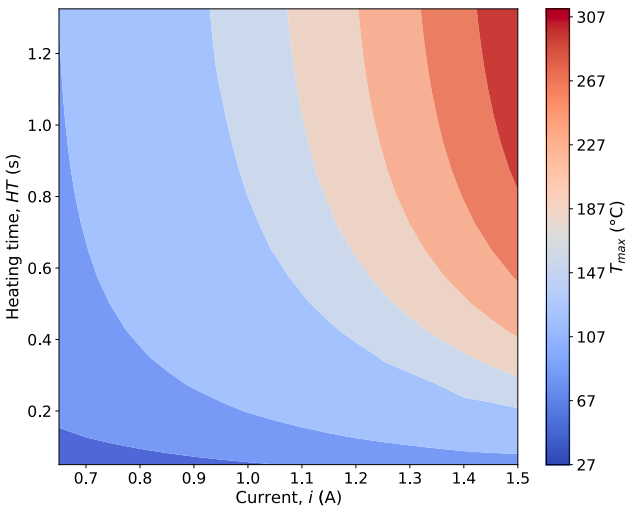

(b) T_{max} isocurves.

Fig. 13. ε_0^{tr} and T_{max} isocurves for different sets of total actuation time for the ∅0.20 mm wire. The color bars at the right side indicate the maximum transformation strain for figure (a) and the maximum reached temperature for figure (b) after ten actuation cycles. (For interpretation of the references to color in this figure legend, the reader is referred to the web version of this article.)

4.4. Impact of the wire diameter

The last part of the parametric analysis investigates the influence of the wire diameter on the activation parameters. In this step, a wire with a diameter of ∅0.50 mm, not previously considered in this study, was selected to more effectively illustrate the broad optimal range of HT and i parameters and their nonlinear interrelationship. In this analysis, only the T_{max} output was investigated. This parameter is sufficient for a direct association between the actuation condition and the actuator functioning. The SMA actuation performance was estimated using two reference quantities: A_f and T_{lim}. A_f is the temperature value used to indicate if the phase transformation is complete and, therefore, if maximum work is generated by the actuator. T_{lim} is an arbitrary value that is chosen as a threshold to guarantee no overheating during the wire operation. If T_{max} is between these two values, minimal actuation performance is ensured. Otherwise, suboptimal work is generated (below A_f) or the actuator may overheat and wear out quickly (above T_{lim}).

A first analysis is carried out under a 200 MPa stress. T_{max} output is shown as a function of HT and i in Fig. 14. The reference temperatures are $A_f = 100\,°C$ and $T_{lim} = 1.2\ \ A_f = 120\,°C$. A_f is estimated from the pseudo diagram in Appendix.

Fig. 14 shows the temperature isocurves and the optimal operating conditions ($A_f < T_{max} < T_{lim}$) in the hatched area. It is noted that the maximum temperature rises in a non-linear way with both HT and i. In addition, at lower current levels, the impact of HT on the temperature is smaller when compared with higher current values. This behavior can be seen more clearly in the hatched area. In this region, the optimized HT values appear in a narrow window at higher currents while for lower currents the HT range is wider.

To confirm that simulations are in agreement with the real thermo-mechanical behavior of the wires, a validation analysis is performed in the following section.

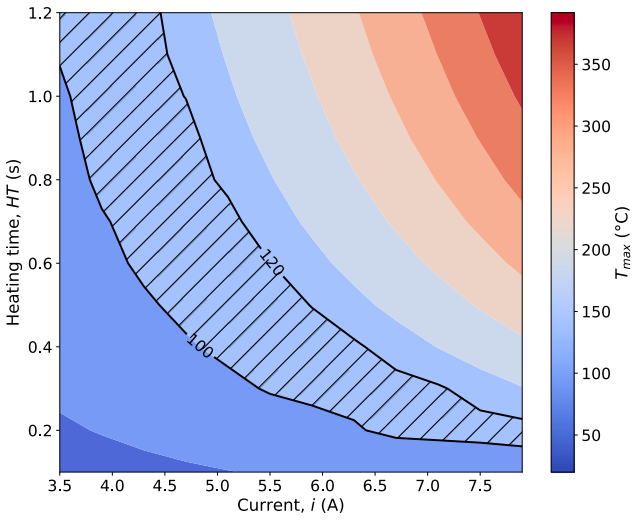

Fig. 14. Maximum temperature isocurves for a ∅0.50 mm wire. The hatched area corresponds to current and heating time conditions in which the maximum temperature is between 100 °C and 120 °C. The color bar at the right side indicates the correspondence between the colors and the maximum temperatures. (For interpretation of the references to color in this figure legend, the reader is referred to the web version of this article.)

4.5. Validation

The goal of this section is to validate the parametric simulations through the comparison of two sets of activation conditions that generate similar strain. For this step, instead of the IR camera, thermocouples attached to the wire surface were used to acquire the temperature. This approach was introduced to address the issue of low thermal resolution observed during the monitoring of thin wires. The primary challenge arose from the curved geometry of the wires, which significantly reduced the detectable surface area available for thermal imaging by the IR camera.

By analyzing again Fig. 13(a), it is noted that different combinations of HT and i result in identical ε_0^{tr}. However, the kinetics of the phase transformation and T_{max} is not the same for each set of parameters. In order to investigate the difference between activation kinetics for an iso-ε_0^{tr} output, a comparison between two sets of HT and i parameters is performed. The investigated set of parameters are $i = 1.0$ A and $HT = 0.65$ s for condition 1 and $i = 1.5$ A and $HT = 0.25$ s for condition 2. For this comparison, simulation results are compared with each other and then with experimental data (Fig. 15).

Fig. 15(a) shows the total strain output measured during an actuation cycle for conditions 1 and 2. The strain evolution during heating is much faster for the higher current condition both in simulations and experiments. By contrast, during cooling, the strain rates seem to be similar in both conditions. The simulation results are in good agreement with the experimental measurements. The differences are due to the smoothness of the strain evolution, which is not fully captured by the proposed model, as already discussed. By comparing the temperature responses from the simulations Fig. 15(b), it is possible to estimate the duration of the phase transformation from the clear changes in the temperature rate. It is evident that the phase transformation duration at the heating stage is much shorter for the higher current condition. This behavior can be analyzed from an energetic point of view: at lower currents, the produced heat rate is smaller, and more time is needed to reach the required temperature to complete the phase transformation.

Regarding the temperature analysis, it is worth noting that despite the efforts to measure the temperature in very thin wires (e.g., ∅0.20 mm), when using thermocouples, another difficulty associated with heat transfer emerged. Due to the thinness of the employed SMA wire, its heated mass was smaller than thermocouple one directly in contact. This disparity, combined with the rapid nature of the Joule heating process resulted in an unbalanced heat state as an insufficient time of heat transfer was available. Consequently, these factors led to delayed/mitigated temperature readings. Despite the low precision of the temperature acquisition, the experimental temperature profile indicates a clear difference between the phase transformation kinetics in the two considered conditions. Such differences (temperature amplitude and rate) are in agreement with the simulations. In this way and despite some disparities, it is concluded that the parametric simulations correctly replicate the effect of the electric parameters on the actuation and phase transformation kinetics.

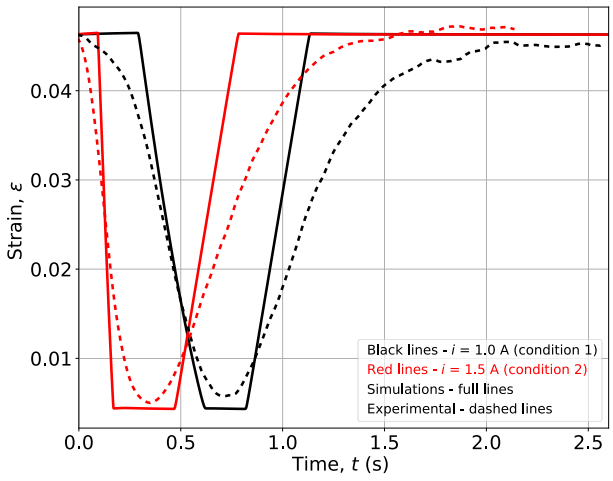

(a) ε evolution.

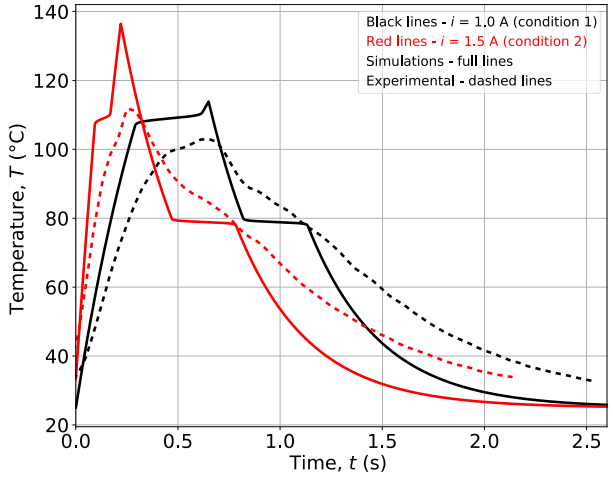

(b) T evolution.

Fig. 15. Comparison between two actuation conditions for ∅0.20 mm wires. The strain evolution is shown on the top and the temperature evolution on the bottom. In both graphs, simulations (full lines) and experimental results (dashed lines) are compared. The colors denote the actuation conditions. (For interpretation of the references to color in this figure legend, the reader is referred to the web version of this article.)

4.6. A practical example of use of the parametric analysis

A practical implementation of the proposed approach is presented here. This example is a guide for HT and i selection at a given stress level (e.g., 230 MPa) for three different wire diameters: 0.50, 0.20 and 0.10 mm. A comparative analysis is performed (as described in

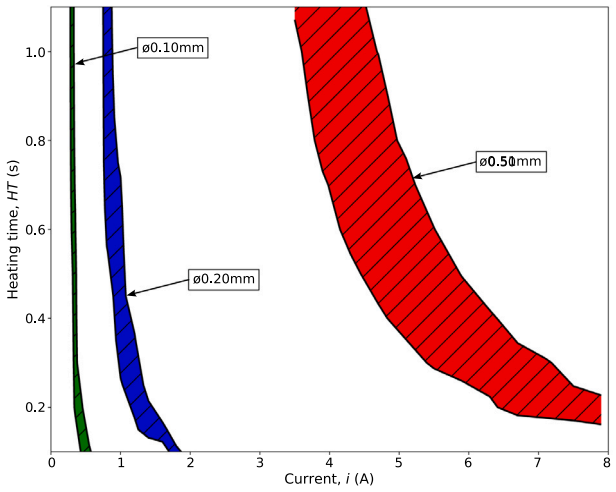

Fig. 16. Optimal electric actuation conditions for three considered wire diameters. The colored areas refers to the electric condition in which the maximum temperature is between 100 °C and 120 °C. Each color corresponds to a given wire diameter. (For interpretation of the references to color in this figure legend, the reader is referred to the web version of this article.)

Section 4.4) for a wide spectrum of HT and i parameters. The most adapted electric actuation conditions are shown with colored areas in Fig. 16. Regarding the operating conditions, significant differences are observed for each wire diameter. Thinner SMA wires are best activated under low currents and in a very narrow range (0.5 A–0.7 A). Thinner wires are much more sensitive to changes in current. On the other hand, thicker wires need higher currents for activation and, a wider set of HT and i produces optimized work. In addition, the parametric analysis on the diameter is in a good agreement with the investigated experimental conditions presented in Section 2. For instance, the optimal range of HT evaluated in Fig. 16 is in correspondence with experimental values observed in Fig. 5 that varies between 0.55 s and 0.80 s for the ∅0.20 mm DN wire.

5. Conclusion

A new strategy for the design of SMA actuators is proposed based on a weak electric-thermo-mechanical coupled model. The approach addresses both the complexity of multiphysical activation and the FF symptoms observed in this kind of devices. The proposed methodology is composed of three steps : SMA composition selection, activation conditions and dimensions and SMA cyclic behavior simulation. The second one, related to the selection of the activation conditions through parametric analysis is the centerpiece of this work.

In an industrial context, total actuation time ($HT + CT$), electrical current, initial actuation strain and maximum temperature can be imposed as specifications for the desired application. In such cases, finding an optimal set of actuation parameters can be very challenging. The proposed parametric approach demonstrated a good agreement with experimental results, accurately simulating strain outputs. However, limitations in temperature monitoring during experiments hindered precise correlations for temperature outputs. Despite these challenges, the observed heat kinetics aligned well with the simulations. To further validate the accuracy of temperature outputs, additional observations with improved temperature monitoring systems are necessary. Finally, the method can be regarded as a useful tool for designers, enabling the exploration of a broad range of operating conditions without the need of extensive experimental testing, which would require demand significant time and resources. In addition, the parametric approach can be adapted to analyze further parameters such as length, voltage or cooling methods.

Although the adopted modeling approach is capable of replicating FF phenomena in SMA actuators, this aspect is not thoroughly analyzed in the current study. Further investigation is required to ensure the reliable operation of actuators throughout their lifespan. To address this limitation, a complementary approach is being developed to integrate with property degradation models to provide robust and lasting solutions for designers. Additionally, the current approach does not incorporate three-dimensional aspects, which should be considered in future work to address more complex SMA actuator geometries.

CRediT authorship contribution statement

Marcos Lopes Leal Júnior: Writing – original draft, Resources, Methodology, Investigation, Formal analysis, Data curation, Conceptualization. **Laurent Pino:** Supervision, Resources, Project administration. **Mahmoud Barati:** Supervision. **Luc Saint-Sulpice:** Supervision. **Laurent Daniel:** Writing – original draft, Supervision, Methodology, Conceptualization. **Shabnam Arbab Chirani:** Visualization, Methodology.

Declaration of competing interest

The authors declare the following financial interests/personal relationships which may be considered as potential competing interests: Laurent Daniel reports was provided by FORVIA. Laurent Daniel reports a relationship with FORVIA that includes: consulting or advisory. If there are other authors, they declare that they have no known competing financial interests or personal relationships that could have appeared to influence the work reported in this paper.

Acknowledgments

The work presented in this paper was supported by the European Commission, through the CPER Eco-SysMer Eu000048.

Appendix. Material parameters identification

The aim of this section is to present the identified material parameters of the 0.38 mm DN wires used in this work. First, the phase transformation temperatures M_s, M_f, A_s, A_f, R_s and R_f of the wires were determined by Differential Scanning Calorimetry (DSC). The results are shown in Fig. A.17. These initial tests allowed defining the testing conditions for further tests. The obtained results for the ASME loading are shown in Fig. A.18. Based on the ASME response, the maximum current transformation strain values (H^{cur}) can be plotted against the stress level. The obtained results are shown in Fig. A.19. Moreover, the phase transformation temperature under different stress levels can also be collected from the ASME tests. From these data, a phase diagram can be established. It is presented in Fig. A.20.

Finally, the convection coefficients (h) were identified from the cooling curves shown in Fig. A.21. These coefficients were evaluated at two different stages where the major thermal exchange took place through forced cooling only (without phase transformation). The first stage is between the hottest temperature and the start of the forward phase transformation and the second is between the end of the phase transformation and the ambient temperature. The coefficients were numbered as 1 and 2, respectively. By comparing different cooling curves, the value of 150 W/m^2 K was identified as the best fit. A summary of the identified data is given in Table A.4.

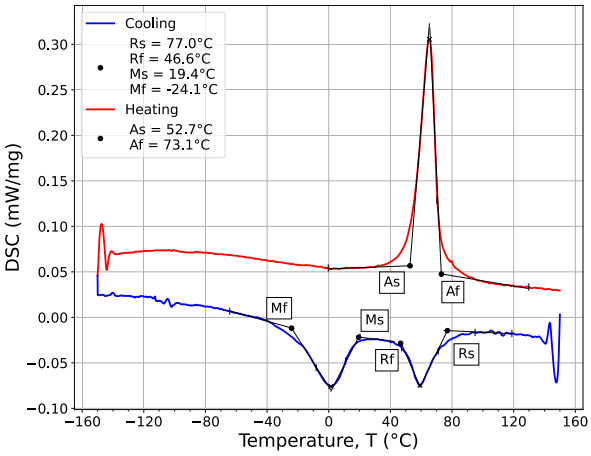

Fig. A.17. DSC test for the studied wires ∅0.38 mm.

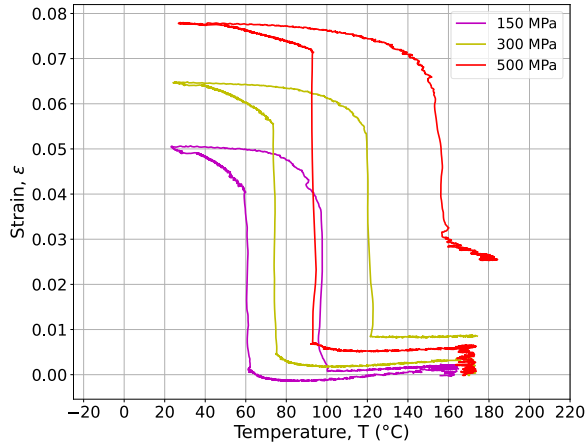

Fig. A.18. Strain-temperature response under ASME loadings for the ∅0.38 mm wires.

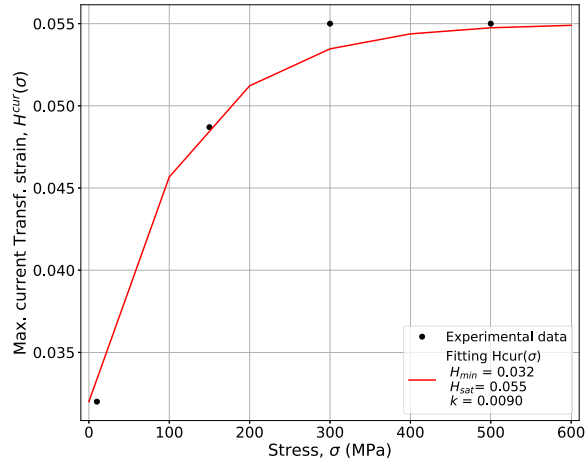

Fig. A.19. Determination of the maximum transformation strain as a function of the applied stress for the studied wires.

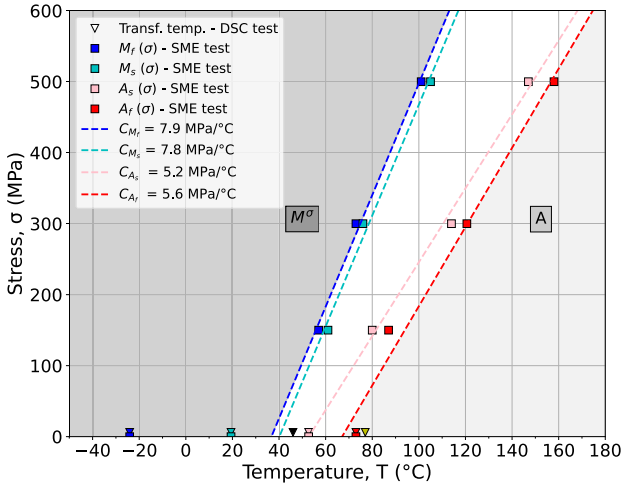

Fig. A.20. Phase diagram. The square markers denote the experimental points evaluated from the AMSE test. The triangle markers denote the experimental points evaluated from the DSC test. The dashed lines denote stress-temperature slopes for the initiation and termination of the phase transformation. The corresponding parameters of the slopes are given in the legend insets.

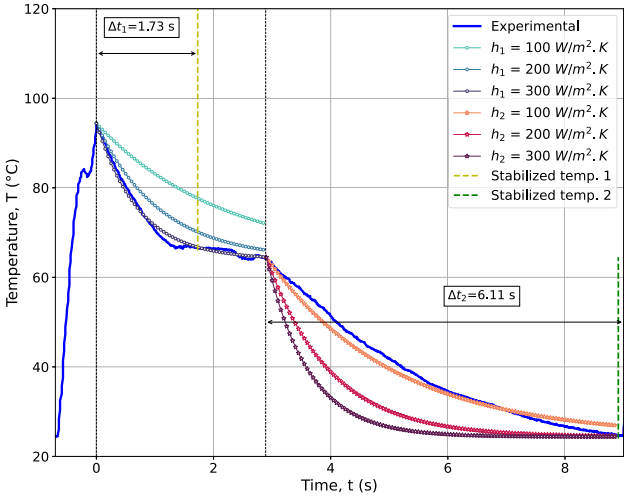

Fig. A.21. Illustration of the convection coefficient identification from a cooling curve. The plain blue curve is the experimental temperature vs. time response. The curves with the circle markers denote the fitting attempts before the phase transformation while the curves with stars markers denote the fitting attempts after the phase transformation. The convection coefficients used at each fitting attempt are given in the legend insets. (For interpretation of the references to color in this figure legend, the reader is referred to the web version of this article.)

Table A.4
Required material parameters for the model.

Model parameter [unit]	Values
Thermoelasticity	
Young's modulus E^A, E^M [GPa]	73, 37 [34]
Thermal expansion coefficients[a] α^A, α^M [K^{-1}]	11E−6, 6E−6 [38]
Phase transformation	
Transformation slopes C^A, C^M [MPa K^{-1}]	6.9, 9.9
Hardening parameters[a] n_1, n_2, n_3, n_4	0.17, 0.27, [29] 0.25, 0.35 [29]
Thermal exchange	
Convection coefficient h [W/m^2 K]	150
Mass density[a] ρ (kg/m^3)	6500 [45]
Specific heat[a] c (J/kg K)	400 [45]
Electrical parameters	
Slope of pure A and M μ_A, μ_M	0.34E−9, 1.34E−9 [34]
Initial resistivity of pure A and M ρ_A, ρ_M	7.07E−7, 7.69E−7 [34]

[a] Taken from the literature.

Data availability

Data will be made available on request.

References

[1] J.M. Jani, M. Leary, A. Subic, Shape memory alloys in automotive applications, 2014, http://dx.doi.org/10.4028/www.scientific.net/AMM.663.248.

[2] R. Casati, F. Passaretti, A. Tuissi, Effect of electrical heating conditions on functional fatigue of thin NiTi wire for shape memory actuators, Procedia Eng. 10 (2011) 3423–3428, http://dx.doi.org/10.1016/j.proeng.2011.04.564.

[3] R.W. Wheeler, D.J. Hartl, Y. Chemisky, D.C. Lagoudas, Modeling of thermo-mechanical fatigue and damage in shape memory alloy axial actuators, in: Behavior and Mechanics of Multifunctional Materials and Composites 2015, Vol. 9432, SPIE, 2015, pp. 140–149, http://dx.doi.org/10.1117/12.2175747.

[4] Y. Chemisky, G. Chatzigeorgiou, P. Kumar, D.C. Lagoudas, A constitutive model for cyclic actuation of high-temperature shape memory alloys, Mech. Mater. 68 (2014) 120–136, http://dx.doi.org/10.1016/j.mechmat.2013.07.020.

[5] G. Scirè Mammano, E. Dragoni, Effect of stress, heating rate, and degree of transformation on the functional fatigue of Ni-Ti shape memory wires, J. Mater. Eng. Perform. 24 (7) (2015) 2709–2719, http://dx.doi.org/10.1007/s11665-015-1561-7.

[6] J.S. Owusu-Danquah, A.F. Saleeb, On the cyclic stability of the thermomechanical behavior of NiTi shape memory cylindrical actuators, Eur. J. Mech. A Solids 64 (2017) 143–159, http://dx.doi.org/10.1016/j.euromechsol.2017.02.005.

[7] V.M. Dornelas, S.A. Oliveira, M.A. Savi, A macroscopic description of shape memory alloy functional fatigue, Int. J. Mech. Sci. 170 (2020) 105345, http://dx.doi.org/10.1016/j.ijmecsci.2019.105345.

[8] M. Leary, S. Huang, T. Ataalla, A. Baxter, A. Subic, Design of shape memory alloy actuators for direct power by an automotive battery, Mater. Des. 43 (2013) 460–466, http://dx.doi.org/10.1016/j.matdes.2012.07.002.

[9] S. Shreekrishna, R. Nachimuthu, V.S. Nair, A review on shape memory alloys and their prominence in automotive technology, J. Intell. Mater. Syst. Struct. 34 (5) (2023) 499–524, http://dx.doi.org/10.1177/1045389X221111547, publisher: SAGE Publications Ltd STM.

[10] B. Fleczok, C. Rathmann, D. Otibar, A. Weirich, B. Kuhlenkötter, Impact of different electrical time-based activations on NiTi shape memory alloys, IOP Conf. Ser.: Mater. Sci. Eng. 216 (1) (2017) 012008, http://dx.doi.org/10.1088/1757-899X/216/1/012008, publisher: IOP Publishing.

[11] M.L.L. Júnior, L. Pino, M. Barati, L. Saint-Sulpice, L. Daniel, S.A. Chirani, Electric resistivity evolution in NiTi alloys under thermomechanical loading: phase proportioning, Elast. Plast. Eff. Smart Mater. Struct. 32 (6) (2023) 065002, http://dx.doi.org/10.1088/1361-665X/accb21, publisher: IOP Publishing.

[12] L. Saint-Sulpice, M. Lakrit, S. Arbab Chirani, S. Calloch, Variation in electric resistivity in metastable alloys during thermomechanical loading: Effects of temperature, elasticity, plasticity and phase transformation, Mech. Mater. 71 (2014) 1–9, http://dx.doi.org/10.1016/j.mechmat.2014.01.004.

[13] P.-A. Gédouin, S.A. Chirani, S. Calloch, Phase proportioning in CuAlBe shape memory alloys during thermomechanical loadings using electric resistance variation, Int. J. Plast. 26 (2) (2010) 258–272, http://dx.doi.org/10.1016/j.ijplas.2009.06.004.

[14] M. Barati, S.A. Chirani, M. Kadkhodaei, L. Saint-Sulpice, S. Calloch, On the origin of residual strain in shape memory alloys: experimental investigation on evolutions in the microstructure of CuAlBe during complex thermomechanical loadings, Smart Mater. Struct. 26 (2) (2017) 025024, http://dx.doi.org/10.1088/1361-665X/aa5745, publisher: IOP Publishing.

[15] M.G. Faulkner, J.J. Amalraj, A. Bhattacharyya, Experimental determination of thermal and electrical properties of Ni-Ti shape memory wires, Smart Mater. Struct. 9 (5) (2000) 632, http://dx.doi.org/10.1088/0964-1726/9/5/307.

[16] J.M. Jani, M. Leary, A. Subic, Fatigue of NiTi SMA–pulley system using Taguchi and ANOVA, Smart Mater. Struct. 25 (5) (2016) 057001, http://dx.doi.org/10.1088/0964-1726/25/5/057001, publisher: IOP Publishing.

[17] A. Rao, A.R. Srinivasa, J.N. Reddy, Design of Shape Memory Alloy (SMA) Actuators, in: SpringerBriefs in Computational Mechanics, Springer International Publishing, 2015, http://dx.doi.org/10.1007/978-3-319-03188-0.

[18] E. Sgambitterra, C. Greco, S. Rodinò, F. Niccoli, F. Furgiuele, C. Maletta, Fully coupled electric-thermo-mechanical model for predicting the response of a SMA wire activated by electrical input, Sensors Actuators A 362 (2023) 114643, http://dx.doi.org/10.1016/j.sna.2023.114643.

[19] S. Rodinò, G. Caroleo, E. Sgambitterra, F. Bruno, M. Muzzupappa, C. Maletta, A multiphysics dynamic model for shape memory alloy actuators, Sensors Actuators A 362 (2023) 114602, http://dx.doi.org/10.1016/j.sna.2023.114602.

[20] L. Fumagalli, F. Butera, A. Coda, SmartFlex® NiTi wires for shape memory actuators, J. Mater. Eng. Perform. 18 (5) (2009) 691–695, http://dx.doi.org/10.1007/s11665-009-9407-9.

[21] P. Shayanfard, L. Heller, P. Šandera, P. Šittner, Numerical analysis of NiTi actuators with stress risers: The role of bias load and actuation temperature, Eng. Fract. Mech. 244 (2021) 107551, http://dx.doi.org/10.1016/j.engfracmech.2021.107551.

[22] X. Qin, X. Zhang, X. Yan, S. Wang, S. Zhang, C. Guo, J. Jiang, B. Zhang, D. Huang, M. Qi, Structural and functional fatigue behavior of Ni49.8Ti50.2 (at. %) wires under various maximum heating temperatures: Experimental and modeling study, Mater. Des. 178 (2019) 107842, http://dx.doi.org/10.1016/j.matdes.2019.107842.

[23] Dynalloy, | Shape Memory Alloy Actuator Wire Manufacturer, DYNALLOY, Inc.

[24] J.J. Amalraj, A. Bhattacharyya, J.J. Amalraj, M.G. Faulkner, Finite-element modeling of phase transformation in shape memory alloy wires with variable material properties, Smart Mater. Struct. 9 (5) (2000) 622, http://dx.doi.org/10.1088/0964-1726/9/5/306.

[25] J. Zhang, Y. Yin, SMA-based bionic integration design of self-sensor–actuator-structure for artificial skeletal muscle, Sensors Actuators A 181 (2012) 94–102, http://dx.doi.org/10.1016/j.sna.2012.05.017.

[26] J.-J. Zhang, Y.-H. Yin, J.-Y. Zhu, Electrical resistivity-based study of self-sensing properties for shape memory alloy-actuated artificial muscle, Sensors 13 (10) (2013) 12958–12974, http://dx.doi.org/10.3390/s131012958, number: 10 Publisher: Multidisciplinary Digital Publishing Institute.

[27] P. Shayanfard, M. Kadkhodaei, A. Jalalpour, Numerical and experimental investigation on electro-thermo-mechanical behavior of NiTi shape memory alloy wires, Iran. J. Sci. Technol. Trans. Mech. Eng. 43 (1) (2019) 621–629, http://dx.doi.org/10.1007/s40997-018-0183-8.

[28] J.M. Jani, S. Huang, M. Leary, A. Subic, Numerical modeling of shape memory alloy linear actuator, Comput. Mech. 56 (3) (2015) 443–461, http://dx.doi.org/10.1007/s00466-015-1180-z.

[29] D.C. Lagoudas, D.A. Miller, L. Rong, P.K. Kumar, Thermomechanical fatigue of shape memory alloys, Smart Mater. Struct. 18 (8) (2009) 085021, http://dx.doi.org/10.1088/0964-1726/18/8/085021, publisher: IOP Publishing.

[30] R. Delville, B. Malard, J. Pilch, P. Sittner, D. Schryvers, Transmission electron microscopy investigation of dislocation slip during superelastic cycling of Ni–Ti wires, Int. J. Plast. 27 (2) (2011) 282–297, http://dx.doi.org/10.1016/j.ijplas.2010.05.005.

[31] Y. Gao, L. Casalena, M.L. Bowers, R.D. Noebe, M.J. Mills, Y. Wang, An origin of functional fatigue of shape memory alloys, Acta Mater. 126 (2017) 389–400, http://dx.doi.org/10.1016/j.actamat.2017.01.001.

[32] Y. Zhang, X. Chai, X. Ju, Y. You, S. Zhang, L. Zheng, Z. Moumni, J. Zhu, W. Zhang, Concentration of transformation-induced plasticity in pseudoelastic NiTi shape memory alloys: Insight from austenite–martensite interface instability, Int. J. Plast. 160 (2023) 103481, http://dx.doi.org/10.1016/j.ijplas.2022.103481.

[33] K. Huang, H. Yin, M. Li, Q. Sun, Grain size dependence of stress-assisted two-way memory effect in Ti-50.04 at.% Ni shape memory alloy, Mater. Sci. Eng. A 856 (2022) 143872, http://dx.doi.org/10.1016/j.msea.2022.143872.

[34] M.L.L. Júnior, L. Pino, M. Barati, L. Saint-Sulpice, L. Daniel, S.A. Chirani, Modeling of functional fatigue of SMA-based actuators under thermomechanical loading and Joule heating, Int. J. Fatigue 179 (2024) 108055, http://dx.doi.org/10.1016/j.ijfatigue.2023.108055.
[35] H. Talebi, H. Golestanian, M. Zakerzadeh, H. Homaei, Thermoelectric heat transfer modeling of shape memory alloy actuators, 2014.
[36] R. Velázquez, E. Pissaloux, Modelling and temperature control of shape memory alloys with fast electrical heating, Int. J. Mech. Control. 13 (2012) 3–10.
[37] J. Strittmatter, P. Gümpel, V. Gheorghita, Shape memory actuators - potentials and specifics of their technical use and electrical activation, J. Achiev. Mater. Manuf. Eng. 55 (2) (2012) 10.
[38] D.C. Lagoudas, P.B. Entchev, Modeling of transformation-induced plasticity and its effect on the behavior of porous shape memory alloys, Part I: constitutive model for fully dense SMAs, Mech. Mater. 36 (9) (2004) 865–892, http://dx.doi.org/10.1016/j.mechmat.2003.08.006.
[39] A. Makhloufi, Y. Aoues, A. El Hami, 5 - Electro-thermo-mechanical modeling, in: A. El Hami, P. Pougnet (Eds.), Embedded Mechatronic Systems, Vol. 2, Elsevier, 2015, pp. 107–150, http://dx.doi.org/10.1016/B978-1-78548-014-0.50005-0.
[40] D.S. of America, Coupled thermal-electrical analysis, 2017.
[41] D. Lagoudas, D. Hartl, Y. Chemisky, L. Machado, P. Popov, Constitutive model for the numerical analysis of phase transformation in polycrystalline shape memory alloys, Int. J. Plast. 32–33 (2012) 155–183, http://dx.doi.org/10.1016/j.ijplas.2011.10.009.
[42] Y. Chemisky, D.J. Hartl, F. Meraghni, Three-dimensional constitutive model for structural and functional fatigue of shape memory alloy actuators, Int. J. Fatigue 112 (2018) 263–278, http://dx.doi.org/10.1016/j.ijfatigue.2018.03.016.
[43] M. Ortiz, J.C. Simo, An analysis of a new class of integration algorithms for elastoplastic constitutive relations, Internat. J. Numer. Methods Engrg. 23 (3) (1986) 353–366, http://dx.doi.org/10.1002/nme.1620230303, _eprint: https://onlinelibrary.wiley.com/doi/pdf/10.1002/nme.1620230303.
[44] R. Holm, Electric Contacts, Springer, Berlin, Heidelberg, 1967, http://dx.doi.org/10.1007/978-3-662-06688-1.
[45] M. Tabesh, B. Lester, D. Hartl, D. Lagoudas, Influence of the Latent Heat of Transformation and Thermomechanical Coupling on the Performance of Shape Memory Alloy Actuators, American Society of Mechanical Engineers Digital Collection, 2013, pp. 237–248, http://dx.doi.org/10.1115/SMASIS2012-8188.

Marcos Lopes Leal Júnior received a Ph.D. degree from the Ecole Nationale d'Ingénieurs de Brest France, in 2024 Currently, he is a R&D Engineer at Safran Aircraft Engines Villaroche, France, contributing to innovations in the field of fatigue of metallic materials. His research interests include material characterization, nonlinear modeling, crack propagation, and correlating modeling with experimental results.

Laurent Pino Qualifications: Ph.D. degree in mechanical engineering from the Ecole Centrale de Nantes, Nantes, France, in 2000. Institutions: Since 2000, Associate professor at ENIB, France and researcher in IRDL (UMR CNRS 6027), Brest France. Expertise: His current research interests include the development and design of mechanical and mechatronic systems using shape memory alloy. He is the co-author of more than 20 publications in international journals and he has more than 15 communications in international conferences. He is the head of ENIB's mechatronics department.

Mahmoud Barati Mahmoud Barati received his Ph.D. in Mechanical Engineering from the University of Western Brittany, Brest, France, in 2017. After completing his Ph.D., he worked as a researcher on the modeling, characterization, and fatigue behavior of smart and conventional materials, focusing on rapid characterization methods. Currently, he is a Senior R&D Engineer at EMITECH Group, Montigny-le-Bretonneux, France, contributing to innovations in the vibrational fatigue behavior of materials. His research interests include material characterization, nonlinear FEM modeling, and the correlation between modeling and experimental results.

Luc Saint-Sulpice Dr. Luc Saint-Sulpice is a materials mechanics researcher specializing in shape memory alloys and fatigue. Based at the Institut de Recherche Dupuy de Lôme (IRDL UMR CNRS 6027) at Brest in France, he investigates the behavior of shape memory alloys through instrumented experimental thermo-mechanical testing, modeling of the cyclic and fatigue behavior, and numerical simulations for metallic materials and especially shape memory alloys.

Laurent Daniel received the Ph.D. degree from the Ecole Normale Superieure de Cachan, Cachan, France, in 2003, and the Habilitation degree in physics from Universite Paris-Sud, Orsay, France, in 2011. Since 2015, he has been a Full Professor with CentraleSupelec, Universite Paris-Saclay, Gif-sur-Yvette, France. His research interests, within the Laboratoire de Genie Electrique et Electronique de Paris, Paris, France, are dedicated to electromechanical and magnetomechanical couplings in materials for electrical engineering applications. He is notably involved in the definition of multiscale methods for the prediction of such coupled phenomena and in the development of dedicated experimental characterization setups.

Shabnam Arbab Chirani After a Ph.D. in mechanical engineering from the University of Technology of Troyes/Compiègne (France) and a first position as a researcher, she has launched a research program on shape memory alloys at ENIB and then at ENSTA Bretagne. She is a specialist in the mechanics of smart materials particularly in shape memory alloys.

Her contribution in the field of shape memory alloys is manifold:

In micro/macro approach, where models are quite physical and possess interesting prediction properties. However, these kinds of models are computationally heavy because of the large number of internal variables they involve and are not easy to use for the dimensioning of mechanical structures.

In macroscopic approach, where models are purely phenomenological, less predictive than the former ones, but permit 3D consideration for massive mechanics structures. This leads to model that can be easily implemented in finite elements codes.

She has early led research in the connection between the two former approaches, and she has proposed contributions to enrich the macroscopic approach from the micro/macro approach. Although her scientific works can be considered as exploratory, she always have addressed the application aspects, in many fields, such as biomedical applications (SMA endodontic instruments dimensioning), mechatronics (development of SMA actuators).

Now she works on the high cycle and low cycle fatigue of these materials. The main objective is to develop smart technics, which permit to reduce the time of characterization or the time of simulations.

She is the co-author of more than 50 publications in international journals and she has more than 100 communications in international conferences.